ACS NANO

www.acsnano.org

ARTICLE

Photovoltaic Performance of PbS Quantum Dots Treated with Metal Salts

Dong-Kyun Ko,[†,‡,¶] Andrea Maurano,[‡,§,¶] Su Kyung Suh,[§] Donghun Kim,[∥,⊥] Gyu Weon Hwang,[∥,#,○] Jeffrey C. Grossman,[∥] Vladimir Bulović,[*,‡] and Moungi G. Bawendi[*,○]

[†]Department of Electrical and Computer Engineering, New Jersey Institute of Technology, Newark, New Jersey 07102, United States

[‡]Department of Electrical Engineering and Computer Science, Massachusetts Institute of Technology, Cambridge, Massachusetts 02139, United States

[§]Advanced Energy Lab, Samsung Advanced Institute of Technology (SAIT)—America, 1 Cambridge Center, Suite 702, Cambridge, Massachusetts 02142, United States

[∥]Department of Materials Science and Engineering, Massachusetts Institute of Technology, Cambridge, Massachusetts 02139, United States

[⊥]Center for Computational Science, Korea Institute of Science and Technology (KIST), Hwarangno 14-gil 5, Seongbuk-gu, Seoul 02792, Republic of Korea

[#]Center for Electronic Materials, Korea Institute of Science and Technology (KIST), Hwarangno 14-gil 5, Seongbuk-gu, Seoul 02792, Republic of Korea

[○]Department of Chemistry, Massachusetts Institute of Technology, Cambridge, Massachusetts 02139, United States

S *Supporting Information*

ABSTRACT: **Recent advances in quantum dot surface passivation have led to a rapid development of high-efficiency solar cells. Another critical element for achieving efficient power conversion is the charge neutrality of quantum dots, as charge imbalances induce electronic states inside the energy gap. Here we investigate how the simultaneous introduction of metal cations and halide anions modifies the charge balance and enhances the solar cell efficiency. The addition of metal salts between QD deposition and ligand exchange with 1,3-BDT results in an increase in the short-circuit current and fill factor, accompanied by a distinct reduction in a crossover between light and dark current density−voltage characteristics.**

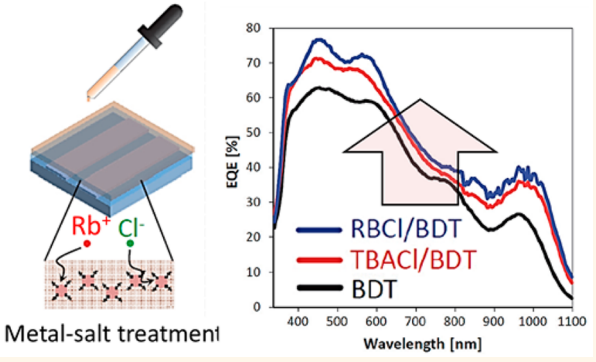

KEYWORDS: *quantum dots, nanocrystals, solar cells, photovoltaics, metal salts*

Quantum dots (QDs) are promising building blocks for optoelectronic devices, as their absorption and emission properties can be tailored simply by adjusting the dot size. The optical gap of lead chalcogenide QDs, for example, can be readily tuned from 0.3 to 1.6 eV and their photoresponse in the near-infrared makes them suitable for a broad range of applications including light-emitting diodes,[1,2] photodetectors,[3,4] and solar cells.[5−8]

QDs have a large portion of atoms situated on the surface.[9] Without passivation, these surface atoms can generate electronic states inside the energy gap[10] which can dominate the electronic properties of the QD film. For solar cell applications, one way to improve the power conversion efficiency (PCE) is to minimize the density of these in-gap states, which degrade the open-circuit voltage (V_{OC}), short-circuit current density (J_{SC}), and the fill-factor (FF). Various ligand strategies have been implemented to improve the surface passivation, including compact organic molecules[11,12] and atomic ligands.[13,14]

For compound semiconductor QDs, charge balance is another key factor to consider in developing high efficiency solar cells. Lead sulfide (PbS) QDs, which are commonly employed in QD solar cells, are composed of two elements with different electronegativities. Charge imbalance originating from the QD's nonstoichiometry and the charges associated with the surface ligands may disturb the overall charge neutrality resulting in electronic in-gap states.[15,16] [In this context, we refer to charge neutrality as the balance among the original

Received: November 14, 2015
Accepted: February 24, 2016
Published: February 24, 2016

DOI: 10.1021/acsnano.5b07186
ACS Nano 2016, 10, 3382−3388

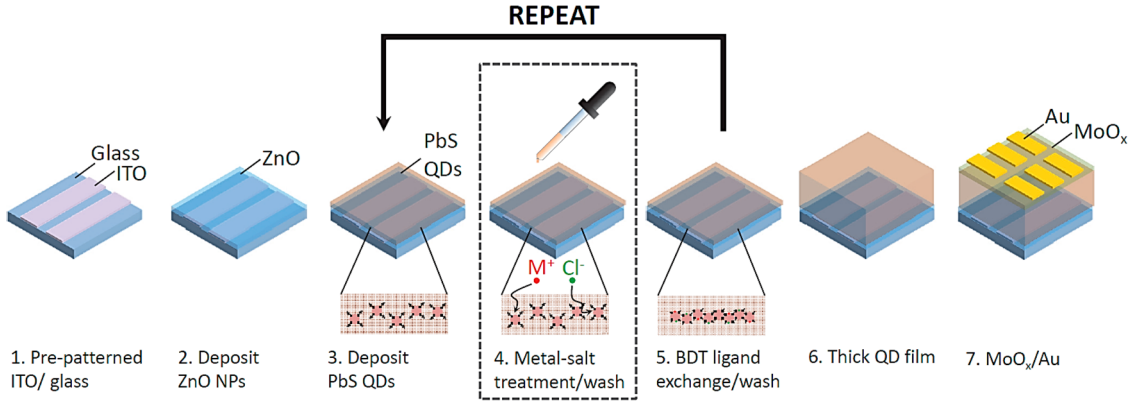

Figure 1. Schematic illustration of QD solar cell fabrication process. For the metal salt treatment, a solution containing metal cations (M^+) and halide anions (Cl^-) is briefly introduced to the QD film (step 4) prior to the BDT treatment.

Table 1. Summary of QD Composition Obtained from As-Deposited PbS QD film (PbS-OLAC), BDT-Treated QD Film (PbS-BDT), TBACl/BDT-Treated QD Film (PbS-TBACl/BDT), and RbCl/BDT-Treated QD Film (PbS-RbCl/BDT) Using WDS and XPS Measurements[a]

	Pb	S total	S-interior	S-ligand	metal	halide	charge balance (R)
PbS-OLAC	1	0.63	0.63	0	0	0	1.59
PbS-BDT	1	1.30	0.75	0.55	0	0	0.98
PbS-TBACl/BDT	1	0.90	0.66	0.15	0	0.24	1.17
PbS-RbCl/BDT	1	0.93	0.81	0.12	0.02	0.35	0.96

[a]All compositions are normalized to Pb. "S total" refers to the total measured sulfur content of the film, "S-interior" refers to S^{2-} in the interior of the QD, and "S-ligand" refers to S^- in the BDT ligands bound to the QD surface. The charge balance (R = positive charge/negative charge) was calculated by taking Pb as +2, S-interior as −2, S-ligand as −1, metal as +1, and halide as −1 charges. According to our definition, the charge balance takes into account only the original oxidation states (formal charge) of the elements listed.

oxidation states of Pb (+2) and S (−2) in a PbS QD. As well-known, the oxidation state is the theoretical charge (formal charge) if all bonds would be ionic, hence, the terminology of charge neutrality. We finally would like to note that in no case (*e.g.*, no stoichiometric QD) our QD film will have a net effective charge because any net effective charge would be promptly neutralized.] Surface ligands used to fabricate high-performance QD solar cells include 1,3-benzenedithiol (BDT),[11] 3-mercaptopropionic acid,[12] and halides,[13,14] which are all negatively charged (X-type ligands). Here, we investigate how the simultaneous introduction of metal cations and halide anions modifies the QD charge neutrality resulting in an increase in PCE from an average of 4.2% for a control device fabricated using 1,3-BDT to an average of 7.3% for a device treated with a mixture of RbCl and 1,3-BDT.

We incorporate the metal halide passivation step into an existing workflow, rather than through complex synthetic steps[7] or chemistry.[17] The Methods section provides a thorough description of the fabrication details, which we briefly describe here. Figure 1 shows a schematic illustration of the QD solar cell fabrication process. A ZnO nanoparticle layer (150 nm) is first deposited on a prepatterned ITO/glass substrate using spin-casting. A PbS QD layer (first excitonic peak in solution of 915 nm) is then deposited *via* sequential spin-casting and ligand exchange (steps 3 and 5 in Figure 1) using 1,3-benzenedithiol (1,3-BDT, 2 mM in acetonitrile)[18] followed by washing with acetonitrile. The spin-casting and ligand exchange steps are repeated until the thickness of the PbS QD layer reaches 220 nm. A molybdenum oxide layer (MoO_x, 5 nm)[13] and Au electrode are deposited by thermal evaporation. For the metal−halide treatment, a solution containing the metal salt (0.025 M in methanol) is introduced to an as-deposited QD film prior to the BDT ligand exchange procedure. Steps 3−5 are repeated until the same thickness of 220 nm is obtained. A similar solid-state treatment approach was recently published by Crisp *et al.* using lead and cadmium halides.[19] In the present study, we use alkali metal cations and halogen, as these metal salts are readily soluble in common solvents such as methanol and ethanol. The uptake of metal chloride salt by PbSe QD was also recently studied by Marshall *et al.* that observed increased stability and performance in solar cells under incorporation of specific metal cations.[20]

To investigate the effects of the surface ligands on photovoltaic performance, we fabricate QD solar cells using PbS QDs treated with 1,3-benzenedithiol (BDT) as a reference, a mixture of tetrabutylammonium chloride and BDT (TBACl/BDT),[21] and a mixture of rubidium chloride and BDT (RbCl/BDT). In contrast to RbCl, which introduces both Rb^+ cations and Cl^- anions, TBACl treatment only introduces Cl^- ligands where bulky ammonium cations are removed during the washing process (see FTIR spectra in Figure S5 in Supporting Information).[13] Thus, comparison of RbCl/BDT and TBACl/BDT devices enables us to study the effect of metal cations on the device performance exclusively. Although we have investigated a series of other alkali metals (see Figure S6 in Supporting Information), no particular trend was observed. Rubidium, which shows the most distinct improvements, will be the focus of the following device studies.

RESULTS AND DISCUSSION

Table 1 summarizes the chemical composition, normalized to Pb, of as-deposited and BDT-, TBACl/BDT-, and RbCl/BDT-treated QD films as determined by wavelength-dispersive X-ray spectroscopy (WDS). WDS data of RbCl only films are

DOI: 10.1021/acsnano.5b07186
ACS Nano 2016, 10, 3382−3388

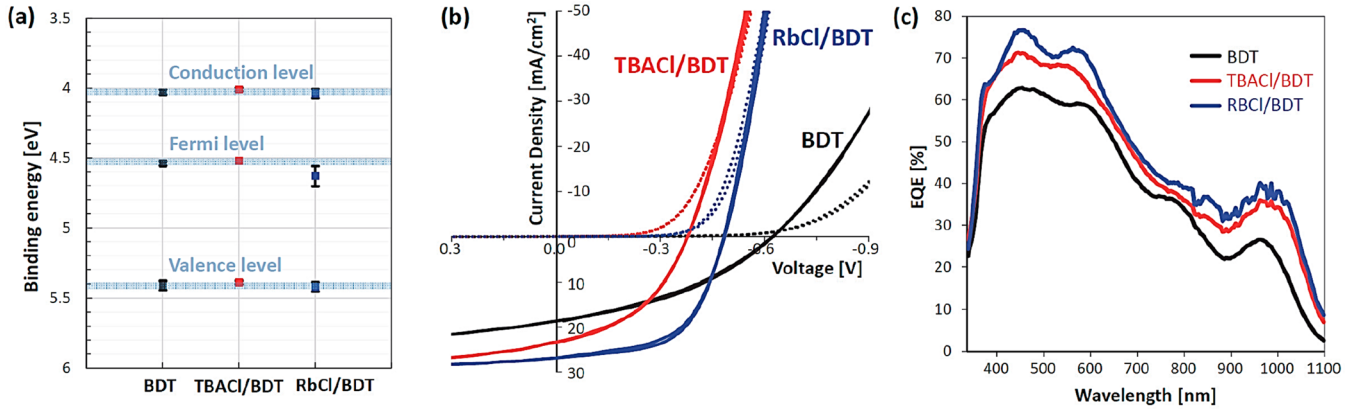

Figure 2. (a) Conduction level, Fermi level, and valence level of BDT- (black), TBACL/BDT- (red), and RbCl/BDT-treated (blue) QD film obtained from UPS measurements. (b) Dark (dotted) and light (solid) $J-V$ characteristics and (c) external quantum efficiency (EQE) of QD solar cells treated with BDT (black), TBACl/BDT (blue), and RbCl/BDT (red).

Table 2. Summary of the Photovoltaic Performance Parameters (Short Circuit Current, J_{SC}; Open-Circuit Voltage, V_{oc}, Fill Factor, FF; Series Resistance, R_S; Shunt Resistance, R_{sh}, Power Conversion Efficiency, η) Obtained from QD Solar Cells Treated with BDT, TBACl/BDT, and RbCl/BDT

	J_{sc} [mA/cm^2]	V_{oc} [V]	FF	R_s [Ω·cm^2]	R_{sh} [Ω·cm^2]	η [%]
BDT	18.4 ± 1.7	0.62 ± 0.03	0.37 ± 0.02	8.4 ± 3.2	88 ± 13	4.2 ± 0.1
TBACl/BDT	22.7 ± 2.3	0.38 ± 0.08	0.42 ± 0.03	2.8 ± 1.8	72 ± 17	3.6 ± 0.3
RbCl/BDT	26.5 ± 1.4	0.48 ± 0.04	0.58 ± 0.02	2.4 ± 1.7	159 ± 10	7.3 ± 0.1

reported in section 3.1 and Table S1 of the Supporting Information. The as-deposited film of PbS QDs coated with oleic acid (PbS-OLAC) shows Pb-rich composition, which is consistent with a previous report.[16,22] For the BDT-treated QD film, additional sulfur introduced from the thiol group generates a sulfur-rich QD film. X-ray photoelectron spectroscopy (XPS) was used to distinguish the S^{2-} in the QD interior from the S^- in the BDT ligands bound to the QD surface (full XPS spectra are given in Figure S4 in Supporting Information).[23] A smaller Pb:S^{2-} ratio for BDT-treated PbS compared to PbS-OLAC indicates that Pb atoms on the surface are etched away during the BDT treatment.[24] The calculated charge balance (R = sum of the positive formal charges/sum of the negative formal charges) for the BDT-treated QD film was 0.98, where R was calculated by taking into account only Pb as +2, S-interior as −2, S-ligand as −1, metal as +1, and halide as −1 formal charges. We point out here that our definition of charge balance refers exclusively to the original oxidation states of the elements listed (formal charge) and not to a net effective charge of the system, as the system will always be neutral overall. TBACl treatment prior to the BDT treatment yields an increase in the ratio of Pb to S^{2-}.[24] Furthermore, we observe a decrease in the fraction of S^- from the BDT ligands, potentially implying that less BDT ligands are attached to the surface due to the presence of Cl^- on the QD surface (see inset in Figure S5 in Supporting Information). The calculated charge balance for TBACl/BDT-treated films (R = 1.17) deviates from unity by a greater amount than that for BDT- (R = 0.98) and RbCl/BDT-treated (R = 0.96) QD films. Treating the QD film with RbCl prior to the BDT results in the smallest Pb to interior S^{2-} ratio.[24] While the QD film has the least S^- from the BDT, the amount of Cl^- increases compared to that of the TBACl-treated QD films. The charge balance calculated from RbCl QD films is R = 0.96, which is shifted closer to unity. The results from the composition analysis indicate that the introduction of Cl^- or Rb^+/Cl^- ions alters the charge balance due not only to the addition of elements with their own formal charge but also to the changes in the number of internal Pb and S atoms.[24] Thus, the resultant QD has the lowest ratio Pb/S-interior which is the closest condition that we have obtained to a stoichiometric dot (as also reported for RbCl only devices in Figure S3 in the Supporting Information).

In Figure 2a, ultraviolet photoelectron spectroscopy (UPS) was performed to investigate the conduction, valence, and Fermi energy levels on the QD films[25] treated with BDT, TBACl/BDT, and RbCl/BDT. There is a negligible change in the conduction and valence levels for all three treatments, which indicates that the energy level alignments at the ZnO/QD and QD/MoO_x interfaces remain unchanged which may otherwise modify the carrier transport and complicate the device analysis. The Fermi energy level, on the other hand, is nearly constant for BDT and TBACl, while an ∼100 meV shift toward the mid-gap is observed for RbCl treated QDs.

The dark and light current density−voltage ($J-V$) characteristics of BDT-, TBACl/BDT-, and RbCl/BDT-treated QD solar cell devices are shown in Figure 2b and summarized in Table 2. The TBACl/BDT and RbCl/BDT devices both demonstrate a higher fill factor (FF) than the reference BDT device. This increase in FF is largely due to a decrease in the series resistance (R_S, calculated from the inverse of the slope of the dark current at ∼1 V) which changes from 8.4, 2.8, to 2.4 Ω·cm^2 for BDT-, TBACl/BDT-, and RbCl/BDT-treated devices, respectively. The TBACl/BDT-treated device demonstrates a lower shunt resistance (R_{sh} = 72.1 Ω·cm^2, calculated from the inverse of the slope at J = 0) than the BDT-treated device (87.7 Ω·cm^2), while the RbCl/BDT-device demonstrates a higher R_{sh} (158.7 Ω·cm^2). The short-circuit current (J_{SC}) is highest for RbCl/BDT treatment and lowest for BDT treatment, while the open-circuit voltage (V_{OC}) is highest for BDT treatment and lowest for TBACl/BDT treatment.

Figure 2c shows the external quantum efficiency (EQE) of the same QD PV devices. The EQE increases progressively

DOI: 10.1021/acsnano.5b07186
ACS Nano 2016, 10, 3382−3388

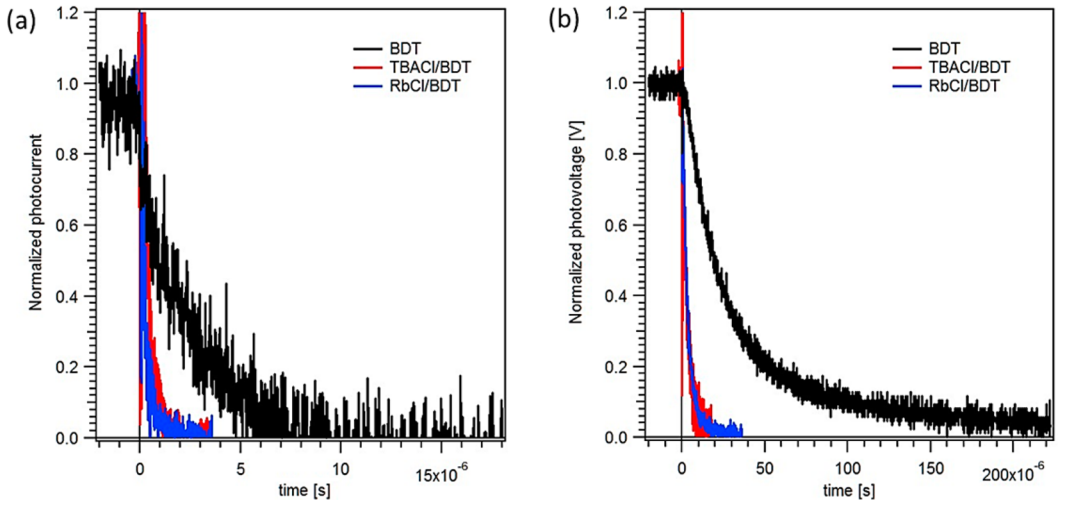

Figure 3. Normalized small perturbation transient (a) photocurrent and (b) photovoltage obtained in QD solar cells devices treated with BDT, TBACl/BDT, and RbCl/BDT.

from BDT treatment to TBACl/BDT treatment to RbCl/BDT treatment. This trend in EQE is in agreement with the trend in J_{SC}, as shown in Figure 2b and the integrated EQE spectra match the J_{sc} from our devices (spectral mismatch factors are 1.1 ± 0.1 for BDT devices, 1.1 ± 0.1 for TBACl/BDT devices, and 1.2 ± 0.1 for RbCl/BDT devices)[26]

Figure 3a shows the transient photocurrent (TPC) data measured under short-circuit conditions. The long transient of BDT-treated and rapid decays of TBACl/BDT- and RbCl/BDT-treated devices imply slow and fast carrier sweep-out, respectively. The results of transient photo voltage (TPV) measurements are shown in Figure 3b. The TPV measurements are performed at open-circuit condition with 1-sun light bias. Compared to the BDT devices, the faster voltage decay of TBACl/BDT and RbCl/BDT devices indicate shorter carrier lifetimes (see also Figure S8 in the Supporting Information).

Computational studies based on *ab initio* density functional theory (DFT) were carried out to understand the electronic structure of the QDs with different ligand exchange treatments. Figure 4 shows the density of state projection of PbS quantum dots constructed using the composition and charge balance obtained from WDS and XPS measurements. The BDT-treated QDs (Figure 4a) with charge balance of R = 0.98, show minimal traps state located inside the energy gap. TBACl/BDT-treated QDs (Figure 4b), which demonstrate the largest stoichiometric imbalance of R = 1.17, exhibit numerous deep trap states near the mid-gap which could function as recombination centers and reduce the V_{OC}. RbCl/BDT-treated QDs (Figure 4c) with charge balance of R = 0.96 show a reduced density of mid-gap states compared to TBACl-treated QDs. The reduced density of mid-gap states for RbCl/BDT-treated QDs is likely responsible for the higher V_{OC} of RbCl/BDT-treated devices than that of TBACl/BDT-treated devices and leads to the highest photovoltaic performance among the ligand-exchange strategies tested here (Figure 2b, Table 2).

We draw three main conclusions from the results described above: (i) TBACl/BDT and RbCl/BDT treatment results in higher electrical conductivity than BDT treatment, leading to an increase in both J_{SC} and FF. (ii) Both TBACl/BDT and RbCl/BDT treatments induce faster recombination than BDT treatment due to the presence of mid-gap states, reducing the V_{OC} compared to that of the BDT-treated devices. However,

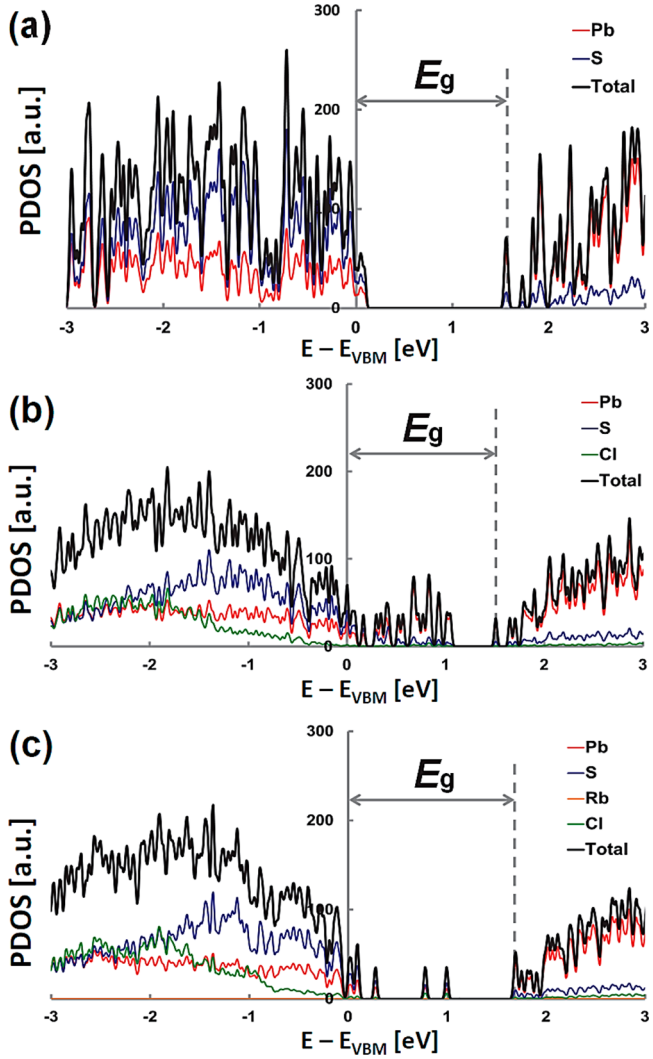

Figure 4. Projected density of state (PDOS) as a function of energy for (a) BDT-, (b) TBACl/BDT-, and (c) RbCl/BDT-treated QDs.

RbCl/BDT treatment results in a lower density of mid-gap states than TBACl/BDT treatment, thereby increasing the V_{OC} compared to that of TBACl/BDT-treated PV devices. (iii) In

DOI: 10.1021/acsnano.5b07186
ACS Nano 2016, 10, 3382–3388

RbCl/BDT devices, the increase in the J_{SC} and FF outweighs the decrease in the V_{OC}, resulting in the highest power conversion efficiency (PCE or η).

J_{SC} and FF Increase in TBACl/BDT and RbCl/BDT Devices. Treating the QD films with Cl^-, either using TBACl or RbCl, increases the electrical conductivity compared to that of the BDT as investigated using the TPC measurements (Figure 3a). In the TPC measurement, the normalized small perturbation photocurrent transients are measured near the short-circuit condition where the internal electric field aid carrier sweep-out with minimal recombination. Under this condition, the rate of carrier sweep-out is proportional to the electrical conductivity of the QD film as demonstrated in section 8 of the Supporting Information and in equation S.8. Hence, a longer transient of BDT and rapid decays of TBACl/BDT and RbCl/BDT devices imply lower and higher conductivities, respectively. The high electrical conductivity of the QD film (rapid carrier extraction) will, first, lead to a high J_{SC}. This is in agreement with the observed increase in the overall spectral response in the EQE (Figure 2c) and the high J_{SC} in TBACl/BDT and RbCl/BDT devices compared to that in the BDT devices.

Second, high electrical conductivity of the QD film will result in a low series resistance (R_S) and is consistent with our observation, as shown in Figure 2b and Table 2. For the shunt resistance (R_{sh}), we speculate that the following mechanism is responsible for the observed trend. As shown in the UPS analysis (Figure 2a), the RbCl/BDT-treated QD film show a downshift (~100 meV) of the Fermi level compared to that of BDT- or TBACl/BDT-treated QD films. Such downshift will establish larger built-in voltage (V_{bi}) when they are made in junction with the ZnO.[18] QD solar cells rely heavily on field-assisted drift for charge carrier collection. Thus, devices with large V_{bi} are likely to collect photogenerated carriers efficiently at short-circuit condition, and applying reverse bias will not assist further charge collection. The expected result will be a saturated reverse current under light which is "measured" as a high shunt resistance (R_{sh}, inverse slope of the photocurrent $J-V$ plot at short-circuit condition) under illumination and, consequently, large FF, as observed in the RbCl/BDT device (Figure 2b and Table 2). Thus, both the decrease in the R_S and increase in the R_{sh} of RbCl/BDT devices result in the highest FF. The FF improvement of TBACl/BDT devices compared to that of the BDT is primary due to the decrease in the R_S.

Another distinct feature we observe in Cl^- treated QD devices (TBACl/BDT and RbCl/BDT devices) is a reduction in the crossover between dark and light $J-V$ characteristics (Figure 2b). Although further studies are warranted, our initial study suggests that photoconductivity of the QD film (not light-induced barrier lowering) is responsible for the crossover behavior (see Figure S7 in Supporting Information).

V_{OC} Decrease in TBACl/BDT and RbCl/BDT Devices. QDs treated either with TBACl/BDT or RbCl/BDT show increase in the carrier recombination compared to those of the BDT as investigated using TPV measurements (Figure 3b). In contrast to the TPC measurements, the transient photovoltage (TPV) is measured at an open-circuit condition where the internal electric field is diminished and significant carrier losses occur due to the recombination. As shown in Figure 3b, rapid decays in the TBACl/BDT and RbCl/BDT devices represent short carrier lifetimes indicative of a faster recombination rate, whereas the long transient in BDT devices indicates slower recombination rate. Since the V_{OC} is related to the amount of recombination in the device, TPV analysis suggests high V_{OC} for BDT and low V_{OC} for TBACl/BDT and RbCl/BDT devices and is consistent with our observation (Figure 2b and Table 2). The rate of recombination measured from TPV and the observed V_{OC} trend are also explained by the DFT calculation results shown in Figure 4. The DFT studies suggest that the charge balance of the QDs has a dominant effect on the mid-gap states, as shown in other studies.[15,27] BDT devices that have charge balance closest to unity have the lowest density of mid-gap states and result in the highest V_{OC} among devices under study. Furthermore, compared to the TBACl/BDT devices, simultaneous introduction of Rb^+ and Cl^- (RbCl/BDT devices) balances the charge closer to unity in the QD film (Table 1), which leads to a reduction in the density of mid-gap states. This leads to slower TPV decay (Figure S8b in Supporting Information) and high V_{OC} observed in RbCl/BDT compared to that of the TBACl/BDT devices.

High Efficiencies in RbCl/BDT Devices. Although we observe faster recombination in TBACl/BDT and RbCl/BDT devices, rapid carrier extraction outweighs the recombination resulting in an increase in the J_{SC} for these devices (Figure 3, Figure S9 in Supporting Information). Both devices thus exhibit improvement in the J_{SC} along with reduction in the V_{OC}. For TBACl/BDT devices, the V_{OC} loss is more than the J_{SC} and FF gain, resulting in a lower PCE compared to that of the reference BDT devices. For RbCl/BDT devices with improved V_{OC} (compared to the TBACl/BDT devices), the J_{SC} and FF gain surpasses the V_{OC} loss and ultimately results in an increased efficiency of 7.3% compared to 4.2% of the reference BDT devices (Figure 2b and Table 2).

CONCLUSIONS

In summary, we have investigated the photovoltaic performance of BDT, TBACl, and RbCl treated QD solar cells. Our results suggest that PbS QD PV devices treated with RbCl/BDT benefits from increased electrical conductivity that increases the J_{SC} and FF. While maintaining the high conductivity, we can reduce the density of trap states through charge balance control. By the simultaneous introduction of Rb^+ and Cl^-, higher V_{OC}, J_{SC}, and FF with 74% improvement in the PCE were achieved. A more careful control of QD charge balance could open up new avenues for optimizing the QD solar cells for high efficiencies.

METHODS

ZnO Nanoparticle Synthesis. ZnO nanoparticles were synthesized using a previously reported method.[28] In brief, 1.10 g of zinc acetate dihydrate (≥98%, Aldrich) was dissolved in 47.5 mL of methanol and the solution was heated to 60 °C. Then, 0.54 g of potassium hydroxide (KOH) dissolved in 24.25 mL of methanol was added dropwise over the course of 3 min while vigorously stirring. After 2 h of reaction, the solution was cooled down to room temperature. The nanoparticles were purified by centrifugation and redissolved in anhydrous methanol. A 40 mg/mL ZnO nanoparticle solution was prepared for thin-film deposition.

PbS QDs Synthesis. PbS QDs with a first excitonic absorption peak at 915 nm were synthesized according to the literature[29] (Figure S1 in the Supporting Information). Lead acetate (11.38 g) was dissolved in 300 mL of 1-octadecene (technical grade, 90%, Aldrich) and 21 mL of oleic acid (technical grade, 90%, Aldrich) at 100 °C. The solution was kept at vacuum overnight and heated to 150 °C under vacuum. Then, 3.15 mL of hexamethyldisilathiane (synthesis grade, Aldrich) diluted with 150 mL of 1-octadecene was swiftly injected to initiate reaction. After the synthesis, the QDs were purified using

DOI: 10.1021/acsnano.5b07186
ACS Nano 2016, 10, 3382−3388

mixture of methanol and butanol, followed by centrifugation. A 20 mg/mL PbS QDs dissolved anhydrous hexane/octane mixture was prepared for thin-film deposition. The entire reaction was performed using standard air-free Schlenk line techniques, and purification steps were done in a nitrogen-filled glovebox.

QD Film Characterizations. UPS spectra were collected using an Omicron ultrahigh vacuum system with a base pressure of 10^{-10} mbar (Figure S2 in the Supporting Information). A glass wafer coated by thermal evaporation with Cr(10 nm)/Au(100 nm) anodes was used as a substrate. PbS QD films were deposited onto the Cr/Au anodes *via* sequential spin-casting and treatment. Four sequential spin-casting cycles result in a QD film thickness of ∼80 nm. PbS QD samples were transported from a nitrogen-filled glovebox (<1 ppm oxygen) into the UPS chamber without exposure to air using a loadlocked transfer system. For the UPS measurement, 21.22 eV illumination was provided using a He(I) discharge lamp. The samples were biased at −5.0 V to ensure accurate determination of the low kinetic energy cutoff, and the chamber pressure during the measurement was 10−7 mbar. The work function (low kinetic energy cutoff) and valence band binding energy (high kinetic energy cutoff) were determined by extrapolating a linear fit of the cutoff region to the *x*-axis. Chemical composition analysis was performed using JEOL JXA-8200 SuperProbe for WDS and PHI Versaprobe II. X-ray Photoelectron Spectrometer was used for XPS analysis. XPS peak fitting was performed using CasaXPS and background is subtracted using Shirley algorithm.[30−32] The standard deviations of the atomic percent measured using WDS were within 0.02−0.61 for all elements. The overall accuracy of the charge balance derived from WDS/XPS is within 0.01. Fourier transform infrared spectroscopy (FTIR) was collected with a Thermo Fisher FTIR6700 Fourier Transform Infrared Spectrometer in Transmission and Attenuated Total Reflection (ATR) mode.

Device Fabrication and Measurements. PbS QD solar cell devices were fabricated as described in the text. Briefly, prepatterened ITO substrates were cleaned with deionized water, acetone, and isopropyl alcohol. A ZnO nanoparticle layer (150 nm) was formed by spin-coating. PbS QD films were prepared from spin-cat PbS QD solution at 2000 rpm for 30 s. The films were subsequently treated with 2 mM 1,3-benzenedithiol (99%, Aldrich) and washed with copious amount of anhydrous acetonitrile. For metal−salt treatment, 0.025 M RbCl (or TBACl) in methanol is briefly introduced (3 s) to an as-deposited QD film, prior to the BDT ligand exchange procedure, followed by methanol washing. These steps were repeated until a thickness of 220 nm (Veeco Dektak 6 M profiler) was reached. Top molybdenum oxide (5 nm) layer and Au electrode (120 nm) are deposited by thermal evaporation using shadow masks.

Current density−voltage (*J*−*V*) characteristics were obtained using a Keithley 6487 Picoammeter and Oriel solar simulator (100 ± 10 mW/cm^2) equipped with Newport 96000 150 W xenon arc-lamp and AM1.5G filter. EQE spectra were measured using a 1000 W xenon lamp with an Acton Spectrapro 300i monochromator. The light was optically chopped and coupled with a Stanford research SR830 DSP lock-in amplifier for photocurrent readout. All the samples were kept in a nitrogen-filled glovebox during the measurement.

Transient photocurrents and photovoltage data were acquired by optically pumping the devices with a Newport laser diode (832 nm) driven by an Agilent 33220 as a square wave function generator. A second light probe source was provided by a solar simulator (Oriel) equipped with Newport 96000 150 W xenon arc-lamp and an AM1.5G filter which intensity was filtered *via* neutral density filters before reaching the device. Transient decays were recorded on a Tektronix TDS 3054B digital oscilloscope. Data acquisition was triggered by the falling front of the square wave.[33−35]

Density Functional Theory Calculations. We performed DFT calculations on neutral quantum dot system using the Vienna *Ab initio* Simulation Packages (VASP) with the generalized gradient approximation of Perdew−Burke−Ernzehof (PBE) for the exchange and correlation functional. The projector-augmented-wave (PAW) method was adopted to describe the core electrons. An energy cutoff of 300 eV and a Monkhorst−Pack k-point sampling 1 × 1 × 1 were used. A large vacuum spacing of >15 Å was used in order to prevent the dot-to-dot interaction. Number of each constituent in a simulated QD was determined to make the overall off-balance be as close to the measured off-balance as possible. Note that the effect of stoichiometry contribution from BDT anionic ligands was considered by having more sulfur atoms within PbS QDs, which reduces the computational burden and allows the simulation of larger QDs. All simulated PbS QDs were fully relaxed using the conjugate gradient method until (i) the energy difference between two consecutive ionic steps is less than 10^{-4} eV, and (ii) the maximum Hellmann−Feynman forces acting on each atom are less than 0.01 eV·Å^{-1}. Details on the QD structures can be found in section 9 of the Supporting Information.

ASSOCIATED CONTENT

Supporting Information

The Supporting Information is available free of charge on the ACS Publications website at DOI: 10.1021/acsnano.5b07186.

Transmission electron microscopy (TEM), optical characterization, ultraviolet photoemission spectroscopy (UPS), Wavelength-dispersive X-ray spectroscopy (WDS), X-ray photoelectron spectroscopy (XPS) and Fourier transform infrared spectroscopy (FTIR) of PbS QD films, together with dark and light *J*−*V* characteristics of QD solar cells treated with different alkali cations, details on the crossover between dark and light *J*−*V* characteristics, semilogarithmic plot of small perturbation transient photocurrent and photovoltage, comparison between photocurrent and photovoltage decays, relation between the lifetime and TPC and conductivity as well as details on QD structures used in DFT calculations (PDF)

AUTHOR INFORMATION

Corresponding Authors

*E-mail: bulovic@mit.edu.
*E-mail: mgb@mit.edu.

Author Contributions

¶D.-K.K. and A.M. contributed equally.

Notes

The authors declare no competing financial interest.

ACKNOWLEDGMENTS

The authors thank P. R. Brown for the UPS measurement and analysis. This work was supported by the Samsung Advanced Institute of Technology (SAIT). D.K. acknowledges support from the Samsung Scholarship Foundation.

REFERENCES

(1) Shirasaki, Y.; Supran, G. J.; Bawendi, M. G.; Bulović, V. Emergence of Colloidal Quantum-Dot Light-Emitting Technologies. *Nat. Photonics* **2012**, *7* (1), 13−23.

(2) Sun, L.; Choi, J. J.; Stachnik, D.; Bartnik, A. C.; Hyun, B.-R.; Malliaras, G. G.; Hanrath, T.; Wise, F. W. Bright Infrared Quantum-Dot Light-Emitting Diodes through Inter-Dot Spacing Control. *Nat. Nanotechnol.* **2012**, *7* (6), 369−373.

(3) Konstantatos, G.; Howard, I.; Fischer, A.; Hoogland, S.; Clifford, J.; Klem, E.; Levina, L.; Sargent, E. H. Ultrasensitive Solution-Cast Quantum Dot Photodetectors. *Nature* **2006**, *442*, 180−183.

(4) Clifford, J. P.; Konstantatos, G.; Johnston, K. W.; Hoogland, S.; Levina, L.; Sargent, E. H. Fast, Sensitive and Spectrally Tuneable Colloidal-Quantum-Dot Photodetectors. *Nat. Nanotechnol.* **2009**, *4* (1), 40−44.

DOI: 10.1021/acsnano.5b07186
ACS Nano 2016, 10, 3382−3388

(5) Gur, I.; Fromer, N. A.; Geier, M. L.; Alivisatos, A. P. Air-Stable All-Inorganic Nanocrystal Solar Cells Processed from Solution. *Science (Washington, DC, U. S.)* **2005**, *310*, 462−465.
(6) Luther, J. M.; Law, M.; Beard, M. C.; Song, Q.; Reese, M. O.; Ellingson, R. J.; Nozik, A. J. Schottky Solar Cells Based on Colloidal Nanocrystal Films. *Nano Lett.* **2008**, *8* (10), 3488−3492.
(7) Ip, A. H.; Thon, S. M.; Hoogland, S.; Voznyy, O.; Zhitomirsky, D.; Debnath, R.; Levina, L.; Rollny, L. R.; Carey, G. H.; Fischer, A.; Kemp, K. W.; Kramer, I. J.; Ning, Z.; Labelle, A. J.; Chou, K. W.; Amassian, A.; Sargent, E. H. Hybrid Passivated Colloidal Quantum Dot Solids. *Nat. Nanotechnol.* **2012**, *7* (9), 577−582.
(8) Chuang, C.-H. M.; Brown, P. R.; Bulović, V.; Bawendi, M. G. Improved Performance and Stability in Quantum Dot Solar Cells through Band Alignment Engineering. *Nat. Mater.* **2014**, *13*, 796.
(9) Borchert, H. *Solar Cells Based on Colloidal Nanocrystals*; Springer International Publishing: Switzerland, 2014.
(10) Gómez-Campos, F. M.; Califano, M. Hole Surface Trapping in CdSe Nanocrystals: Dynamics, Rate Fluctuations, and Implications for Blinking. *Nano Lett.* **2012**, *12* (9), 4508−4517.
(11) Brown, P. R.; Lunt, R. R.; Zhao, N.; Osedach, T. P.; Wanger, D. D.; Chang, L.-Y.; Bawendi, M. G.; Bulović, V.; Bulovic, V. Improved Current Extraction from ZnO/PbS Quantum Dot Heterojunction Photovoltaics Using a MoO(3) Interfacial Layer. *Nano Lett.* **2011**, *11* (7), 2955−2961.
(12) Barkhouse, D. A. R.; Debnath, R.; Kramer, I. J.; Zhitomirsky, D.; Pattantyus-Abraham, A. G.; Levina, L.; Etgar, L.; Gratzel, M.; Sargent, E. H. Depleted Bulk Heterojunction Colloidal Quantum Dot Photovoltaics. *Adv. Mater.* **2011**, *23*, 3134−3138.
(13) Tang, J.; Kemp, K. W.; Hoogland, S.; Jeong, K. S.; Liu, H.; Levina, L.; Furukawa, M.; Wang, X.; Debnath, R.; Cha, D.; Chou, K. W.; Fischer, A.; Amassian, A.; Asbury, J. B.; Sargent, E. H. Colloidal-Quantum-Dot Photovoltaics Using Atomic-Ligand Passivation. *Nat. Mater.* **2011**, *10* (10), 765−771.
(14) Ning, Z.; Ren, Y.; Hoogland, S.; Voznyy, O.; Levina, L.; Stadler, P.; Lan, X.; Zhitomirsky, D.; Sargent, E. H. All-Inorganic Colloidal Quantum Dot Photovoltaics Employing Solution-Phase Halide Passivation. *Adv. Mater.* **2012**, *24* (47), 6295−6299.
(15) Kim, D.; Kim, D.-H.; Lee, J.-H.; Grossman, J. C. Impact of Stoichiometry on the Electronic Structure of PbS Quantum Dots. *Phys. Rev. Lett.* **2013**, *110* (19), 196802.
(16) Hwang, G. W.; Kim, D.; Cordero, J. M.; Wilson, M. W. B.; Chuang, C.-H. M.; Grossman, J. C.; Bawendi, M. G. Identifying and Eliminating Emissive Sub-Bandgap States in Thin Films of PbS Nanocrystals. *Adv. Mater.* **2015**, *27* (30), 4481−4486.
(17) Bae, W. K.; Joo, J.; Padilha, L. A.; Won, J.; Lee, D. C.; Lin, Q.; Koh, W.; Luo, H.; Klimov, V. I.; Pietryga, J. M. Highly Effective Surface Passivation of PbSe Quantum Dots through Reaction with Molecular Chlorine. *J. Am. Chem. Soc.* **2012**, *134* (49), 20160−20168.
(18) Ko, D.-K.; Brown, P. R.; Bawendi, M. G.; Bulović, V. P-I-N Heterojunction Solar Cells with a Colloidal Quantum-Dot Absorber Layer. *Adv. Mater.* **2014**, *26* (28), 4845−4850.
(19) Crisp, R. W.; Kroupa, D. M.; Marshall, A. R.; Miller, E. M.; Zhang, J.; Beard, M. C.; Luther, J. M. Metal Halide Solid-State Surface Treatment for High Efficiency PbS and PbSe QD Solar Cells. *Sci. Rep.* **2015**, *5*, 9945.
(20) Marshall, A. R.; Young, M. R.; Nozik, A. J.; Beard, M. C.; Luther, J. M. Exploration of Metal Chloride Uptake for Improved Performance Characteristics of PbSe Quantum Dot Solar Cells. *J. Phys. Chem. Lett.* **2015**, *6*, 2892−2899.
(21) Balazs, D. M.; Dirin, D. N.; Fang, H.-H.; Protesescu, L.; ten Brink, G. H.; Kooi, B. J.; Kovalenko, M. V.; Loi, M. A. Counterion-Mediated Ligand Exchange for PbS Colloidal Quantum Dot Superlattices. *ACS Nano* **2015**, *9*, 11951.
(22) Moreels, I.; Fritzinger, B.; Martins, J. C.; Hens, Z. Surface Chemistry of Colloidal PbSe Nanocrystals. *J. Am. Chem. Soc.* **2008**, *130* (45), 15081−15086.
(23) Klem, E. J. D.; MacNeil, D. D.; Levina, L.; Sargent, E. H. Solution Processed Photovoltaic Devices with 2% Infrared Monochromatic Power Conversion Efficiency: Performance Optimization and Oxide Formation. *Adv. Mater.* **2008**, *20*, 3433−3439.
(24) Anderson, N. C.; Hendricks, M. P.; Choi, J. J.; Owen, J. S. Ligand Exchange and the Stoichiometry of Metal Chalcogenide Nanocrystals: Spectroscopic Observation of Facile Metal-Carboxylate Displacement and Binding. *J. Am. Chem. Soc.* **2013**, *135* (49), 18536−18548.
(25) Brown, P. R.; Kim, D.; Lunt, R. R.; Zhao, N.; Bawendi, M. G.; Grossman, J. C.; Bulović, V. Energy Level Modification in Lead Sulfide Quantum Dot Thin Films through Ligand Exchange. *ACS Nano* **2014**, *8* (6), 5863−5872.
(26) Shrotriya, V.; Li, G.; Yao, Y.; Moriarty, T.; Emery, K.; Yang, Y. Accurate Measurement and Characterization of Organic Solar Cells. *Adv. Funct. Mater.* **2006**, *16* (15), 2016−2023.
(27) Voznyy, O.; Zhitomirsky, D.; Stadler, P.; Ning, Z.; Hoogland, S.; Sargent, E. H. A Charge-Orbital Balance Picture of Doping in Colloidal Quantum Dot Solids. *ACS Nano* **2012**, *6* (9), 8448−8455.
(28) Pacholski, C.; Kornowski, A.; Weller, H. Self-Assembly of ZnO: From Nanodots, to Nanorods. *Angew. Chem., Int. Ed.* **2002**, *41*, 1188−1191.
(29) Hines, M. A.; Scholes, G. D. Colloidal PbS Nanocrystals with Size-Tunable Near-Infrared Emission: Observation of Post-Synthesis Self-Narrowing of the Particle Size Distribution. *Adv. Mater.* **2003**, *15* (21), 1844−1849.
(30) Moulder, J. F.; Stickle, W. F.; Sobol, P. E.; Bomben, K. D. *Handbook of X-Ray Photoelectron Spectroscopy*; Perkin−Elmer Corporation: Eden Prairie, MN, 1992.
(31) National Institute of Standards and Technology. NIST X-ray Photoelectron Spectroscopy Database, Version 4.1 http://srdata.nist.gov/xps/ (accessed May 20, 2002).
(32) Beamson, G.; Briggs, D. High Resolution XPS of Organic Polymers: The Scienta ESCA300 Database. *J. Chem. Educ.* **1993**, *70* (1), A25.
(33) O'Regan, B. C.; Scully, S.; Mayer, A. C.; Palomares, E.; Durrant, J. The Effect of Al2O3 Barrier Layers in TiO2/Dye/CuSCN Photovoltaic Cells Explored by Recombination and DOS Characterization Using Transient Photovoltage Measurements. *J. Phys. Chem. B* **2005**, *109*, 4616−4623.
(34) Shuttle, C. G.; O'Regan, B.; Ballantyne, A. M.; Nelson, J.; Bradley, D. D. C.; de Mello, J.; Durrant, J. R. Experimental Determination of the Rate Law for Charge Carrier Decay in a Polythiophene: Fullerene Solar Cell. *Appl. Phys. Lett.* **2008**, *92*, 093311.
(35) Maurano, A.; Hamilton, R.; Shuttle, C. G.; Ballantyne, A. M.; Nelson, J.; O'Regan, B.; Zhang, W. M.; McCulloch, I.; Azimi, H.; Morana, M.; Brabec, C. J.; Durrant, J. R. Recombination Dynamics as a Key Determinant of Open Circuit Voltage in Organic Bulk Heterojunction Solar Cells: A Comparison of Four Different Donor Polymers. *Adv. Mater.* **2010**, *22*, 4987−4992.

DOI: 10.1021/acsnano.5b07186
ACS Nano 2016, 10, 3382−3388